cIAP1/2 Antagonism Induces Antigen-Specific T Cell–Dependent Immunity

Katherine S. Ventre,* Kevin Roehle,*,†,‡ Elisa Bello,*,§ Aladdin M. Bhuiyan,*,§ Tamara Biary,*,§ Stephanie J. Crowley,* Patrick T. Bruck,* Max Heckler,*,† Patrick J. Lenehan,*,† Lestat R. Ali,*,§,¶ Courtney T. Stump,*,†,§ Victoria Lippert,* Eleanor Clancy-Thompson,*,† Winiffer D. Conce Alberto,*,† Megan T. Hoffman,*,† Li Qiang,*,† Marc Pelletier,‡ James J. Akin,‡ Michael Dougan,§,¶ and Stephanie K. Dougan*,†

Checkpoint blockade immunotherapy has failed in pancreatic cancer and other poorly responsive tumor types in part due to inadequate T cell priming. Naive T cells can receive costimulation not only via CD28 but also through TNF superfamily receptors that signal via NF-κB. Antagonists of the ubiquitin ligases cellular inhibitor of apoptosis protein (cIAP)1/2, also called second mitochondria-derived activator of caspases (SMAC) mimetics, induce degradation of cIAP1/2 proteins, allowing for the accumulation of NIK and constitutive, ligand-independent activation of alternate NF-κB signaling that mimics costimulation in T cells. In tumor cells, cIAP1/2 antagonists can increase TNF production and TNF-mediated apoptosis; however, pancreatic cancer cells are resistant to cytokine-mediated apoptosis, even in the presence of cIAP1/2 antagonism. Dendritic cell activation is enhanced by cIAP1/2 antagonism in vitro, and intratumoral dendritic cells show higher expression of MHC class II in tumors from cIAP1/2 antagonism-treated mice. In this study, we use in vivo mouse models of syngeneic pancreatic cancer that generate endogenous T cell responses ranging from moderate to poor. Across multiple models, cIAP1/2 antagonism has pleiotropic beneficial effects on antitumor immunity, including direct effects on tumor-specific T cells leading to overall increased activation, increased control of tumor growth in vivo, synergy with multiple immunotherapy modalities, and immunologic memory. In contrast to checkpoint blockade, cIAP1/2 antagonism does not increase intratumoral T cell frequencies. Furthermore, we confirm our previous findings that even poorly immunogenic tumors with a paucity of T cells can experience T cell–dependent antitumor immunity, and we provide transcriptional clues into how these rare T cells coordinate downstream immune responses. ***The Journal of Immunology*****, 2023, 210: 991–1003.**

Drugs targeting the inhibitor of apoptosis proteins (IAPs) are currently in clinical trials, but how these drugs work, what combination therapies would be most effective, and which cancer types might be most responsive are largely unknown. The IAP family is defined by the presence of a baculovirus inhibitory repeat (BIR) domain, which was initially identified by its ability to bind and inhibit caspases. IAPs are now known to play a much broader role in cell signaling, growth, and survival (1). The cellular IAPs (cIAPs) are critical regulators of both classical and alternative NF-κB signaling, functioning downstream of multiple TNF family receptors (1). Endogenously, IAPs are regulated by the mitochondrial protein second mitochondria-derived activator of caspases (SMAC), which binds to the IAP baculovirus inhibitory repeat domain through a tetrapeptide motif. Small-molecule SMAC mimetics including LCL-161, also known as IAP antagonists, have been developed as cancer therapeutics (2–5). In preclinical testing, these drugs were found to induce cancer cell death through activation of TNF-α–dependent apoptosis in only a subset of tumors (2, 4–6). LCL-161 binds to the cIAPs, leading to a conformational change in cIAP1 that enables autoubiquitination and degradation, followed by downstream alterations in NF-κB signaling (2, 4–7). LCL-161 does not merely inhibit cIAP1/2, it leads to complete loss of the proteins by proteasomal degradation, giving the drug a long effective half-life.

Although IAP antagonists may affect tumor cell–intrinsic NF-κB signaling in some tumor types, their most pronounced effects are on

*Department of Cancer Immunology and Virology, Dana-Farber Cancer Institute, Boston, MA; †Department of Immunology, Harvard Medical School, Boston, MA; ‡Novartis Institute for Biomedical Research, Cambridge, MA; §Division of Gastroenterology, Department of Medicine, Massachusetts General Hospital, Boston, MA; and ¶Department of Medicine, Harvard Medical School, Boston, MA

ORCIDs: 0000-0002-7675-7355 (K.S.V.); 0000-0001-7695-2567 (E.B.); 0000-0002-6665-0108 (S.J.C.); 0000-0002-8278-3904(P.T.B.); 0000-0003-3213-5068 (M.H.); 0000-0003-2673-1592 (L.R.A.); 0000-0001-8114-8186 (C.T.S.); 0000-0002-4097-9861 (W.D.C.A.); 0000-0003-0907-9977 (M.T.H.); 0000-0002-2354-177X (L.Q.); 0000-0002-0131-0620 (J.J.A.); 0000-0002-2263-363X (S.K.D.).

Received for publication August 30, 2022. Accepted for publication January 24, 2023.

S.K.D. was supported by the Hale Center for Pancreatic Cancer Research, the Ludwig Center at Harvard, the Dana-Farber Cancer Institute/Novartis Institutes for BioMedical Research Program in Drug Discovery, Cancer Moonshot (Misión contra el Cáncer) Grant U01 CA224146-01, and by National Institute of Allergy and Infectious Diseases Grant 1R01AI158488-01. M.H. was supported by Deutsche Forschungsgemeinschaft Project 398222819. E.C.-T. and P.J.L. were supported by National Cancer Institute Grant T32CA207021. L.Q. was supported by a SITC-Bristol Myers Squibb Postdoctoral Cancer Immunotherapy Translational Fellowship. M.D. was supported by National Cancer Institute Grant R01CA177684, the National Institutes of Health Mentored Clinical Scientist Development Award/National Institute of Diabetes and Digestive and Kidney Diseases Grant 1K08DK114563-01, the Fariborz Maseeh Award for Innovative Medical Education, and the Peter and Ann Lambertus Family Foundation. M.D. and S.K.D. were supported by the Melanoma Research Alliance and American Cancer Society.

The RNA sequencing datasets presented in this article have been submitted to the Gene Expression Omnibus (https://www.ncbi.nlm.nih.gov/geo/query/acc.cgi?acc=GSE222095) under accession number GSE222095.

Address correspondence and reprint requests to Dr. Stephanie K. Dougan, Dana-Farber Cancer Institute, 450 Brookline Avenue, Boston, MA 02215. E-mail address: stephanie_dougan@dfci.harvard.edu

The online version of this article contains supplemental material.

Abbreviations used in this article: BMDC, bone marrow–derived DC; cDC1, conventional type 1 DC; cDC2, conventional type 2 DC; cIAP, cellular IAP; DC, dendritic cell; IAP, inhibitor of apoptosis protein; PBST, PBS with Tween 20; PDAC, pancreatic ductal adenocarcinoma; MDSC, myeloid-derived suppressor cell; TRP1, tyrosinase-related protein 1.

the generation of antitumor immunity. Work from our group and others demonstrated that the cIAPs complex with TNFR-associated factor (TRAF)2 and TRAF3 downstream of many TNF family receptors, including the immune costimulatory receptors CD40, OX40, 4-1BB, and GITR (1, 8–13). The cIAPs constitutively ubiquitinate NIK, thereby preventing p100 processing to p52, and regulate the switch between canonical and noncanonical NF-κB signaling. Loss of cIAP1/2 results in accumulation of NIK and increased production of p52/RelB target genes, including chemokines and cytokines such as IL-2, TNF-α, and GM-CSF. In B cells the cIAPs are required for effective CD40 signaling, whereas loss of cIAP1 in B cells triggers a growth signal similar to activation of BAFF receptor (9, 10). We demonstrated that the IAPs play a critical role in regulating T cell activation. IAP antagonists have no effect on T cells in the absence of TCR stimulation, but they can deliver a strong costimulatory signal to CD4, CD8, and NKT cells in both mice and humans (8, 11). We further found that IAP antagonist treatment of mice could augment antitumor responses to melanoma in combination with either a vaccine or an NKT cell agonist (8, 11). Subsequent work has supported these initial findings, demonstrating augmented naive T cell responses in IAP antagonist-treated cells, as well as in cells expressing a dominant negative cIAP1 RING domain mutant (14–16). Two publications have demonstrated synergy between LCL-161 and PD-1 antagonists in models of myeloma and glioblastoma (17, 18). In both myeloma and pancreatic cancer models, macrophage activation resulted in enhanced phagocytic uptake of tumor cells (12, 18); in pancreatic cancer, cIAP1/2 antagonism enabled effective antitumor immune responses to MHC class I–negative tumors and combination therapy with blockade of the phagocytic "don't eat me" ligand CD47 (12).

We previously reported T cell–dependent activation of macrophages in poorly immunogenic pancreatic cancer (12). To better understand how cIAP1/2 antagonism leads to activated T cells and to demonstrate the Ag specificity of the ensuing responses, we used multiple models of pancreatic cancer that span a wide range of immunogenicity and represent the full spectrum of immune phenotypes observed in humans. We first present data from highly immunogenic KPC.1 pancreatic tumors that are well infiltrated by CD8 T cells and respond to combination checkpoint blockade (19). We also evaluate growth in the liver of the poorly immunogenic pancreatic cell line 6694c2 (20). Although 6694c2 pancreatic tumors do not elicit a robust T cell response, we also engineered these cells to express the self-antigen tyrosinase-related protein 1 (TRP1) and adoptively transferred traceable TRP1-specific CD8 T cells (21). Finally, we evaluated cIAP1/2 antagonism in our most refractory model of pancreatic cancer, a live-passage organoid system that enriches for tumor-specific T cells in the inoculum. In all cases, we show that cIAP1/2 antagonism effectively controls tumor growth in a T cell–dependent fashion and combines with multiple T cell–directed therapies.

Materials and Methods

Cell lines

KPC.1 cells derived from a LSL-Kras^{G12D};p53+/floxed;Pdx-cre mouse were a gift from Dr. Anirban Maitra (MD Anderson). The KPCY cell line 6694C2 was a gift from Dr. Ben Stanger (University of Pennsylvania) and was previously described (20). B16-OVA cells were a gift from Dr. Robert Manguso and were previously described (22). C2VTRP1 cells were generated using parental 6694c2 cells engineered to express a TRP1 transgene. Cells were transfected with Lipofectamine stem reagent and used according to the manufacturer's protocol. Cells were selected with Geneticin for successful transfection, and gene insertion was confirmed by immunoblot. Cells were cultured at 37°C in a humidified incubator with 5% CO_2. RPMI 1640 medium was supplemented with 10% FBS, 2 mmol/l L-glutamine, 1% penicillin/streptomycin, 1% MEM nonessential amino acids, 1 mmol/l sodium pyruvate, and 0.1 mmol/l 2-ME. Cells used for in vitro experiments were cultured with 500 nM LCL-161 or 0.1% DMSO (vehicle). Cytokines were purchased from PeproTech (IFN-γ, TNF-α, TRAIL) and used at the indicated concentrations. Cells used for in vivo experiments had been passaged for <2 mo, were negative for known mouse pathogens, and were implanted at >95% viability.

Mice

All animal protocols were approved by the Dana-Farber Cancer Institute Committee on Animal Care (protocol nos. 14-019 and 14-037) and are in compliance with the National Institutes of Health/National Cancer Institute ethical guidelines for tumor-bearing animals. The following mouse strains were purchased from The Jackson Laboratory: C57BL/6 (000664), μMT$^{-/-}$ (002249), Batf3$^{-/-}$ (013755), TCRα$^{-/-}$ (002116), β2m$^{-/-}$ (002087), RAG2$^{-/-}$ (008449). TRP1^{high};CD45.1 mice were generated by us as previously described (21, 23) and bred in-house.

Orthotopic pancreatic tumors

Orthotopic surgeries were performed as described (24). Briefly, mice were anesthetized with a ketamine/xylazine mixture, shaved on the left flank, and the surgical site was cleaned with ethanol and betadine. An incision was made in the skin and peritoneum, and the pancreas was externalized with forceps. KPC.1 cells were resuspended in PBS and mixed 1:1 by volume with Matrigel (Corning) for a total of 100,000 cells per 30 μl. The cell suspension was kept on ice and drawn into a chilled insulin syringe. Cells were then injected into the tail of the pancreas, and a bubble was observed. Mice that showed signs of leakage were removed from the experiment. The pancreas was left external to the body cavity for 1 min with the mice on a warming pad to solidify the Matrigel. The pancreas was then reinserted, the peritoneum was sutured with one stitch of absorbable suture, and the skin was stapled with a sterile wound clip. Mice were given analgesia (meloxicam and ropivacaine) and monitored postsurgery according to protocols approved by the Dana-Farber Institutional Animal Care and Use Committee. Mice were sacrificed at 21 d postsurgery unless otherwise indicated. Tumors were weighed at the time of sacrifice.

Liver metastasis model

Tumor cells were injected as previously described (25). Briefly, the spleen was cut in half after placing two surgical ligating clips in the center. Tumor cells were injected in one half. The splenic blood vessels were cauterized, and the injected hemispleen was removed. Mice were monitored closely and sacrificed on day 18 postinjection. Liver weights of noninjected healthy mice were used to set baseline liver weight and weight change of liver as readouts for metastatic tumor burden.

Live-passage organoid model

M8 organoids were a gift from Dr. David Tuveson and were previously described (24). Organoids were seeded initially in Matrigel domes in organoid media in 24-well plates. Domes were then digested with trypsin, washed in PBS, and resuspended in PBS at 1 dome per 15 μl and mixed 1:1 by volume with Matrigel (Corning). This mixture was implanted orthotopically into C57BL/6 mice as described above. After 8 wk, pancreatic masses could be felt by palpation. Tumors were harvested and digested to a single-cell suspension by mincing and incubating in RPMI 1640 containing collagenase and anti-trypsin at 37°C for 1 h. Tumors were filtered through a 40-μm cell strainer, washed with PBS, and centrifuged. The resulting cell pellet containing tumor debris and infiltrating immune cells was resuspended in PBS and Matrigel and reimplanted orthotopically into C57BL/6 mice. This first mouse-to-mouse passage was defined as passage 1. Experiments shown here were conducted using tumors from passages 2 to 23.

Tumor infiltrate analysis

Pancreatic tumors were excised, weighed, minced, and incubated in RPMI 1640 containing collagenase and anti-trypsin at 37°C for 1 h. Tumors were filtered through a 40-μm cell strainer, washed with PBS, and centrifuged. The resulting cell pellet containing tumor debris and infiltrating immune cells was resuspended in FACS buffer (PBS with 2% FCS) and stained with a master mix of Abs. Cells were incubated with staining mix for 30 min at 4°C, washed once in PBS, and resuspended in 1% formalin prior to analysis on either a spectral flow cytometer (Sony SP6800) or an LSRFortessa flow cytometer (BD Biosciences). Flow cytometry Abs used in this study were purchased from BioLegend and included anti-CD45 (30-F11), anti-CD4 (RM4-5), anti-CD8 (53-6.7), anti-NK1.1 (PK136), anti-CD103 (2E7), anti-Ly6C (1A8), anti–I-A/I-E (M5/114.5.2), anti-F4/80 (BM8), anti–Siglec-F (E50-2440), anti-CD11b (M1170), anti-CD11c (N418), anti-GR1 (RB6-8C5), and anti–H-2K^b (AF6-88.5).

In vivo treatments

LCL-161 was provided by Novartis Pharmaceuticals and solubilized in 0.1 N HCl and diluted in sodium acetate buffer to a final concentration of 10 mg/ml and pH 4.3. LCL-161 was administered by oral gavage at 75 mg/kg every 3 d starting at day 4 after tumor inoculation unless otherwise indicated.

Mice received depleting Abs on the day of tumor inoculation and then every 3 d until sacrifice. Depleting Abs were given i.p. at 100 μg/mouse. Anti–PD-L1 (clone 10F.9G2), anti–CTLA-4 (clone 9D9), or anti–PD-1 (clone 29F.1A12) was administered i.p. at 200 μg/mouse starting at day 4 postinoculation every 3 d. All Abs were purchased from Bio X Cell, including anti-CD4 (GK1.5) and anti-CD8 (2.43).

For adoptive transfer of TRP1^{high} CD8 T cells, spleens and lymph nodes of TRP1^{high};CD45.1 mice were harvested and CD8 T cells were isolated by negative selection on magnetic beads (STEMCELL Technologies). T cells were suspended in 150 μl of sterile PBS per mouse, and 1 million CD8 T cells per mouse were transferred by tail vein injection to recipient hosts bearing C2VTRP1 tumors.

Generation of bone marrow–derived myeloid-derived suppressor cells

Bone marrow was flushed from C57BL/6 mouse femurs and erythrocytes lysed in hypotonic buffer. Ten million cells were plated in a 10-cm dish with 10 ml of RPMI 1640 medium supplemented with 20 ng/ml each G-CSF, GM-CSF, and IL-6. After 3 d of culture, a mixture of granulocytic CD11b$^+$ Ly6G^{high}Ly6C^{low} (40%) and monocytic CD11b$^+$Ly6G^{low}Ly6C^{high} (60%) myeloid-derived suppressor cells (MDSCs) was obtained and used in in vitro T cell suppression assays.

Generation of bone marrow–derived dendritic cells

Bone was flushed from C57BL/6 mouse femurs and erythrocytes lysed in hypotonic buffer. Then, 50,000 cells were plated per well of a 48-well tissue culture–treated plate in 500 μl of RPMI 1640 medium supplemented with 20 ng/ml GM-CSF and IL-4. After 3 and 6 d of culture, additional GM-CSF/IL-4–containing medium was added. After day 7, dendritic cells (DCs) were confirmed by flow cytometry to be >80% CD11c$^+$MHC class II$^+$ and used for in vitro assays. Cells were dissociated by treatment with 1× TrypLE (Life Technologies) for 10–30 min at 37°C and vigorous pipetting. In some cases, LPS (100 ng/ml) was added to bone marrow–derived DC (BMDC) cultures.

ELISPOT

Tumor-specific T cells were identified by ELISPOT as previously described (26). ELISPOT plate (BD Biosciences) was treated with sterile-filtered 70% ethanol before being washed three times with sterile 1× PBS. IFN-γ capture Ab (BD Biosciences, no. 551881) was plated and the plate was sealed and left to incubate at 4°C overnight. Positive control wells were also plated with anti-CD3ε (BioLegend, no. 100340). The plate was washed three times with sterile PBS and blocked with 10% (v/v) FBS in PBS overnight at 4°C. IFN-γ–stimulated 6694c2, Panc02, M8, or KPC.1 cells were plated, except in the unstimulated and positive control wells. Draining lymph nodes or spleen was excised from treated mice as indicated and macerated to form a single-cell suspension. Lymph node cells (one-third of lymph node per well) were plated on top of preplated tumor cells with human IL-2 (PeproTech), and positive control wells also received anti-CD28 (BioLegend, no. 102116). The plate was incubated at 37°C for 24 h before being washed with sterile water followed by PBS with Tween 20 (PBST). IFN-γ detection Ab (BD Biosciences, no. 551881) was added, and the plate was incubated for 2 h at room temperature. Wells were washed with PBST, and streptavidin-HRP (BD Biosciences) was added. The plate was incubated for 1 h at room temperature before being washed with PBST and PBS. 3-Amino-9-ethylcarbazole chromogen (AEC) substrate (BD Biosciences) was added and the plate was developed. The plate was dried and analyzed.

Tumor confluency

A Celigo Image Cytometer (Nexcelom 200-BFFL-5c) was used to monitor cell growth of cell lines in conditioned media over 4 d. Cells were seeded in 96-well plates and treated with 0.1 ng/ml TNF-α or 1 ng/ml TNF-α in combination with 500 nM LCL-161. Confluence was measured.

Bulk RNA sequencing and data analysis

CD45$^+$CD4$^+$ or CD45$^+$CD8$^+$ cells were sorted by FACS from orthotopic live-passage M8 organoid pancreatic tumors implanted in TCRα$^{-/-}$ mice treated with vehicle or LCL-161 for 12 d. Total RNA was prepared using a Qiagen RNeasy kit according to the manufacturer's protocol. Library construction and Illumina sequencing were performed by the Dana-Farber Cancer Institute Molecular Genomics Core Facility. Reads were trimmed for Illumina adapter sequences using cutadapt and aligned using STAR (v2.7.3a) to the GRCm38 genome. Feature counting was done in R using the package Rsubread allowing for fractional counting of multimapping reads. Genes with <10 reads across all samples were discarded, and the remaining genes were analyzed for differential expression using the package DESeq2. Gene set enrichment analysis was performed using the fgsea package.

Data and code availability

Bulk RNA sequencing datasets are available in GEO under accession number GSE222095 (https://www.ncbi.nlm.nih.gov/geo/query/acc.cgi?acc=GSE222095). Code used to analyze data are available at https://github.com/douganlab/Roehle.

Statistical analysis

All tumor weight and tumor infiltrates data are presented as mean with SD error bars unless otherwise noted. Significance was determined using a two-sided Mann–Whitney *U* test to compare ranks, without assuming Gaussian distribution. GraphPad Prism software was used to analyze data. Exact *p* values are reported in each figure panel. The sample size (*n*) for each group can be determined by the number of individual data points shown in each graph, which are all independent biological replicates. For some figures, data from multiple experiments were combined for presentation in the same graph. In these cases, tumor weights were normalized to the average of the control (vehicle) group within each experiment and data are presented as normalized tumor weights on the *y*-axis.

Results

cIAP1/2 antagonism is effective in vivo in an immunogenic model of pancreatic cancer

To test the role of cIAP1/2 antagonism in a T cell–dependent model of pancreatic cancer, we used KPC.1 cells, which contain model neoantigens derived from strain differences between the donor KPC mouse and C57BL/6 mice and are most reflective of the rare microsatellite instability–high subset of human pancreatic ductal adenocarcinoma (PDAC) (19, 27). In vitro, KPC.1 cells show induction of alternate NF-κB signaling in response to cIAP1/2 antagonism, as demonstrated by increased nuclear p52 after 24 h of culture with LCL-161 (Fig. 1A). However, in vitro growth rates of KPC.1 cells were not affected by exposure to LCL-161 either alone or in combination with TNF-α, IFN-γ, or TRAIL (Fig. 1B, Supplemental Fig. 1A, 1B). IFN-γ treatment increased expression of MHC class I, MHC class II, and PD-L1 on KPC.1 cells as expected, but this IFN-dependent increase was not affected by exposure to LCL-161 (Supplemental Fig. 1C). Thus, cIAP1/2 antagonism does not affect in vitro growth or response to cytokine signaling in KPC.1 cells.

We next implanted KPC.1 cells orthotopically into the pancreas of immune-competent C57BL/6 mice and treated the mice with LCL-161 every 3 d by oral gavage. In this context, cIAP1/2 antagonism significantly decreased tumor burden, implicating the host microenvironment in tumor regression (Fig. 1C). To ascertain potential differences in cytokine and chemokine production that might affect the composition of the immune microenvironment, we profiled KPC.1 cells in vitro and orthotopic tumors ex vivo by cytokine bead array (Fig. 1D, 1E). Cultured KPC.1 cells produced several cytokines and chemokines that accumulated to >10 pg/ml in vitro, including GM-CSF, IL-6, VEGF, KC, LIF, CCL2, CXCL2/3, and CXCL10. Of these, several were significantly increased by cIAP1/2 antagonism, including GM-CSF, KC, LIF, CCL2, and CXCL10 (Fig. 1D). In vivo, several additional cytokines and chemokines were present that were not detected in cell culture supernatants, suggesting that IL-5, TNF-α, eotaxin, and CXCL9 are most likely produced by stromal cells in the pancreatic tumor microenvironment. In vivo, cIAP1/2 antagonism increased the concentrations of multiple cytokines and chemokines, including GM-CSF, M-CSF, IL-1α, IL-1β, IL-6, VEGF, KC, LIF, and CXCL2/3 (Fig. 1E). T cell–derived cytokines IL-2 and IFN-γ were negligible in these samples, leading to an overall picture of cIAP1/2 antagonism increasing predominantly innate inflammatory cytokines and myeloid cell–recruiting chemokines.

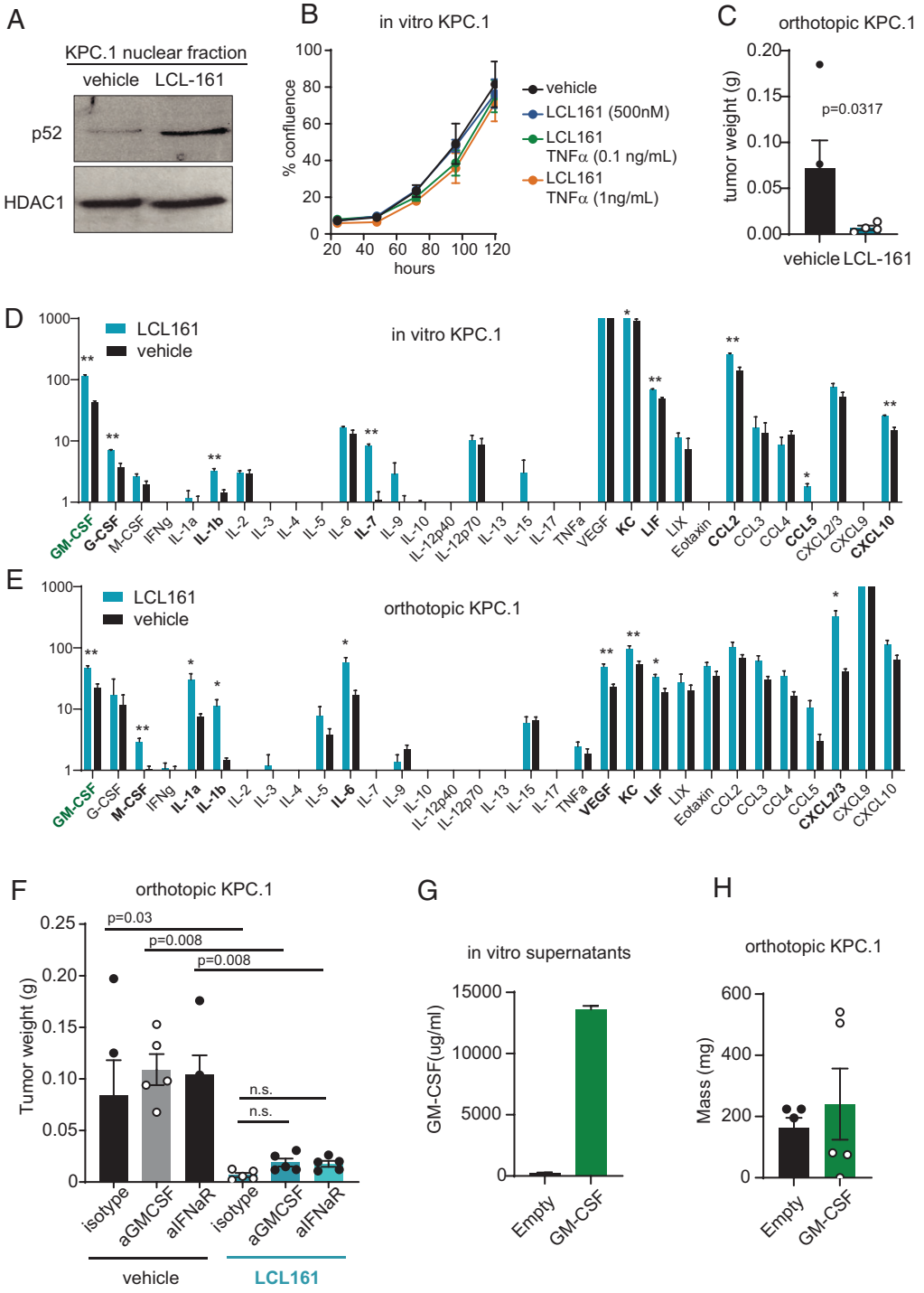

FIGURE 1. Pancreatic tumor cells are resistant to cIAP1/2 antagonism in vitro but sensitive in vivo. (**A**) KPC.1 cells were cultured with vehicle or 500 nM LCL-161 in RPMI 1640 complete medium for 24 h prior to fractionation and protein lysis of the nuclear fraction. Immunoblotting for nuclear p52 and HDAC1 are shown. (**B**) KPC.1 cells were seeded at low density in media containing 500 nM LCL-161 or vehicle and recombinant mouse TNF-α at the indicated concentrations. Cell confluence was measured by imaging cytometry (Celigo). (**C**) C57BL/6 mice were inoculated orthotopically with 50,000 KPC.1 cells suspended in Matrigel and dosed with vehicle or LCL-161 (75 mg/kg) by oral gavage every 3 d starting on day 4. Tumors were harvested 21 d after inoculation and weights are reported. (**D**) KPC.1 cells were seeded at 50% confluency and cultured for 48 h with and without 500n M LCL-161. Culture supernatants were collected and subjected to cytokine bead array analysis (Eve Technologies). $n = 5$ per group. (**E**) KPC.1 cells were suspended in Matrigel and implanted orthotopically in the pancreas of C57BL/6 mice and treated with LCL-161 or vehicle every 3 d starting at day 4 post-inoculation. Tumors were harvested at day 12, after mice received three total doses of LCL-161. Tumors were lysed in RIPA buffer and subjected to cytokine bead array analysis (Eve Technologies). Values were normalized to total protein concentration of each sample. $n = 5$ per group. (**F**) C57BL/6 mice were inoculated orthotopically with 50,000 KPC.1 cells suspended in Matrigel and dosed with vehicle or LCL-161 (75 mg/kg) by oral gavage every 3 d starting on day 4. Mice were also treated with isotype control, anti–GM-CSF, or anti-IFNaR Abs twice weekly (150 μg/mouse, i.p.). Tumors were harvested 21 d after inoculation and weights are reported. (**G**) KPC.1 cells were transduced with empty vector or GM-CSF overexpression vector. Culture supernatants were analyzed by ELISA for GM-CSF. (**H**) KPC.1 cells from (G) were implanted orthotopically into C57BL/6 mice. Tumors were harvested 21 d later. Error bars are SEM throughout. A Mann–Whitney *t* test was used for comparison between two groups. ANOVA with multiple comparisons was used when more than two groups were present. In (D) and (E), $*p < 0.05$, $**p < 0.01$.

We explored two cytokines in more detail, namely type I IFN (not measured in our cytokine bead array) and GM-CSF, which was consistently increased by cIAP1/2 antagonism. Previous reports of cIAP1/2 antagonism in glioblastoma suggested a role for type I IFN as demonstrated by loss of therapeutic efficacy in mice treated with anti-IFNaR (18). To test whether type I IFN was necessary for a response of orthotopic KPC.1 tumors to cIAP1/2 antagonism, we treated mice with either isotype control or IFNaR blocking Ab and

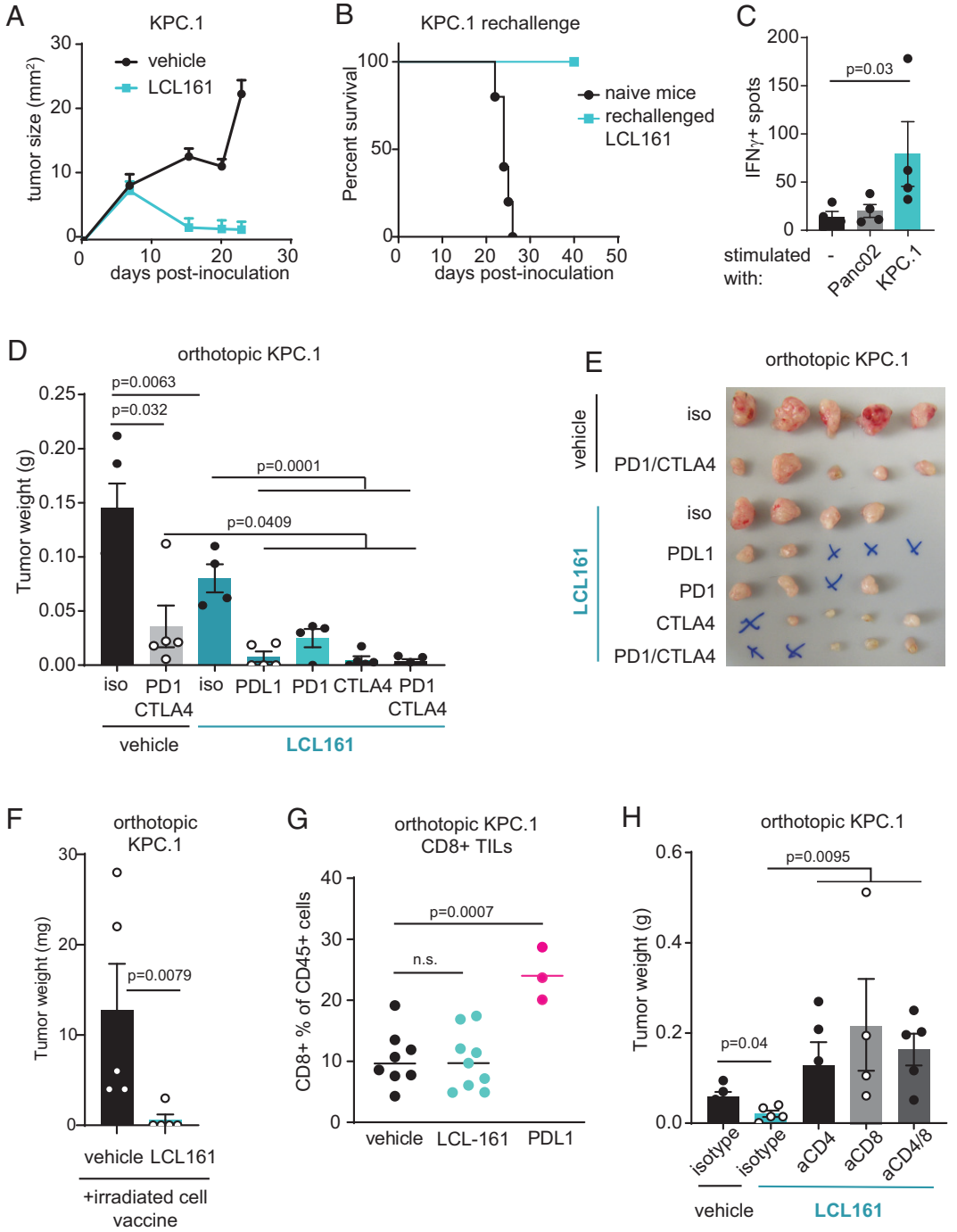

FIGURE 2. cIAP1/2 antagonism synergizes with checkpoint blockade in immunogenic PDAC. (**A**) KPC.1 cells (150,000) were inoculated s.c. into C57BL/6 mice that were treated with LCL-161 (75 mg/kg) or vehicle by oral gavage every 3 d starting on day 5 postinoculation. (**B**) Cured mice from (A) were rechallenged with 300,000 KPC.1 cells. $n = 4$. (**C**) Spleen cells of $n = 4$ rechallenged mice were restimulated with KPC.1 cells or a different PDAC cell line (Panc02) and analyzed by IFN-γ ELISPOT. (**D**) KPC.1 cells were suspended in Matrigel and implanted orthotopically in the pancreas of C57BL/6 mice and treated with LCL-161 and the indicated checkpoint blockade Abs (200 μg/mouse, twice weekly). Tumors were analyzed at day 21. Results are representative of two independent experiments. (**E**) Photograph of tumors from (D). An "X" indicates no tumor was detected. (**F**) KPC.1 cells were irradiated and injected s.c. into C57BL/6 mice that were also inoculated orthotopically with 50,000 live KPC.1 cells suspended in Matrigel. Mice were dosed with vehicle or LCL-161 (75 mg/kg) by oral gavage every 3 d starting on day 4. Tumors were harvested at day 21. Results are representative of three independent experiments. (**G**) Orthotopic tumors from mice treated as in (D) were digested and analyzed by flow cytometry for CD8 T cell infiltrates. Values are out of total $CD45^+$ cells. Results are representative of five independent experiments. (**H**) C57BL/6 mice were inoculated orthotopically with 50,000 KPC.1 cells in Matrigel and treated with vehicle or LCL-161 (75 mg/kg) by oral gavage every 3 d starting on day 4. Mice were also treated with depleting Abs to CD4, CD8, both CD4 and CD8, or isotype control (150 μg/mouse) twice weekly starting on the day of tumor inoculation. Tumors were harvested at day 18. Error bars are SEM throughout. A Mann–Whitney *t* test was used for statistical analysis.

found that blockade of type I IFN signaling did not prevent the efficacy of LCL-161 in vivo (Fig. 1F). Similarly, blockade of GM-CSF, the cytokine most consistently upregulated by LCL-161 and an important differentiation factor for monocyte-derived DCs, did not affect LCL-161–mediated reduction in tumor burden (Fig. 1F). GM-CSF plays pleiotropic roles in cancer (28). As a component of irradiated cell-based vaccines (29, 30), GM-CSF can induce strong tumor regressions, but local production of GM-CSF by pancreatic tumor cells has been reported to induce MDSC formation and accelerate tumor growth (31–33). To test whether GM-CSF would be growth promoting or growth reducing in the highly immunogenic KPC.1 model, we engineered KPC.1 cells to secrete GM-CSF (Fig. 1G). When implanted orthotopically, GM-CSF–overexpressing tumors grew to similar sizes as control tumors (Fig. 1H), strongly indicating that the 2-fold increase in GM-CSF induced by LCL-161 is not sufficient to account for the dramatic reductions in tumor burden.

cIAP1/2 antagonism is T cell–dependent and synergizes with checkpoint blockade

We hypothesized that cIAP1/2 antagonism augmented tumor-specific T cell responses in immunogenic PDAC, potentially inducing Ag-specific memory. To test this, we inoculated C57BL/6 mice s.c. with KPC.1 cells and treated the mice with LCL-161 after tumors were palpable. KPC.1 tumors fully regressed in most mice, and cured mice were refractory to rechallenge, demonstrating immunologic memory (Fig. 2A, 2B). Spleens of rechallenged mice contained tumor-specific T cells as shown by IFN-γ ELISPOT (Fig. 2C). Orthotopic KPC.1 tumors are partially sensitive to anti–CTLA-4/anti–PD-1, indicative of a baseline endogenous antitumor T cell response and defining these tumors as immunogenic. To enhance this endogenous T cell response, we treated mice with a combination of LCL-161 and checkpoint blockade and found that combinations employing either anti–CTLA-4 or anti–PD-1/anti–PD-L1 led to complete responses, with an overall curative response in 7 of 19 mice (Fig. 2D, 2E). We further tested the combination of cIAP1/2 antagonism with an irradiated tumor cell vaccine, which resulted in four of five tumor-free mice in the treated group compared with none of five tumor-free mice in the group receiving an irradiated cell vaccine alone (Fig. 2F).

Blockade of the PD-1 pathway results in an expansion of CD8 T cells in responding tumors, and indeed we observed an increase in intratumoral CD8 T cells in mice with orthotopic KPC.1 tumors treated with anti–PD-L1 (Fig. 2G). In contrast, LCL-161 treatment did not significantly increase the frequency of intratumoral CD8 T cells (Fig. 2G), suggesting a different mechanism of action from checkpoint blockade. To test whether T cells were required for the efficacy of cIAP1/2 antagonism, we used depleting Abs to CD4, CD8, or both in mice implanted with orthotopic KPC.1 tumors (Fig. 2H). Surprisingly, tumor growth was accelerated in mice depleted of either CD4 or CD8 T cells, and treatment with cIAP1/2 antagonism was ineffective in this setting. Thus, we conclude that both CD4 and CD8 T cells are required for the activity of cIAP1/2 antagonism in immunogenic pancreatic cancer.

Pancreatic cancer metastasizes most frequently to the liver, where the immunosuppressive microenvironment of the liver niche promotes tumor growth. To evaluate whether cIAP1/2 antagonism could reduce tumor burden in the liver, we used a hemispleen injection model whereby tumor cells are seeded into the liver via the portal venous circulation (25). cIAP1/2 antagonism was significantly effective at reducing tumor burden in both hemispleen-injected KPC.1 tumors and the more poorly immunogenic 6694c2 pancreatic tumor cell line (Fig. 3A, 3B). Similar to our results in the orthotopic setting, depletion of CD4 and CD8 T cells reduced the efficacy of cIAP1/2 antagonism against liver metastasis (Fig. 3C), indicating that the response is T cell–dependent.

cIAP1/2 antagonism enhances DC activation but has negligible effects on MDSCs

DCs are key to the priming of naive T cells (34). We had previously reported that cIAP1/2 antagonism mimics signaling through TNFR superfamily members and has effects on both newly primed T cells as well as on DCs, which increased expression of MHC class II and production of IL-12 upon exposure to cIAP1/2 antagonism (8). To better profile the activation state of DCs, we generated BMDCs and compared expression of costimulatory ligands MHC class II and CCR7 upon exposure to LCL-161, LPS, or the combination (Fig. 4A, 4E). cIAP1/2 antagonism increased surface expression of MHC class II, CD80, CD86, and OX40L comparably to LPS, with additive increases observed in BMDCs cultured with the combination of LCL-161 and LPS. Surface PD-L1 was also increased in all treatment groups (Fig. 4F). CCR7 was upregulated by LPS as expected, but curiously failed to be induced by LCL-161 treatment. Thus, cIAP1/2 antagonism in DCs appears to increase expression of MHC class II and

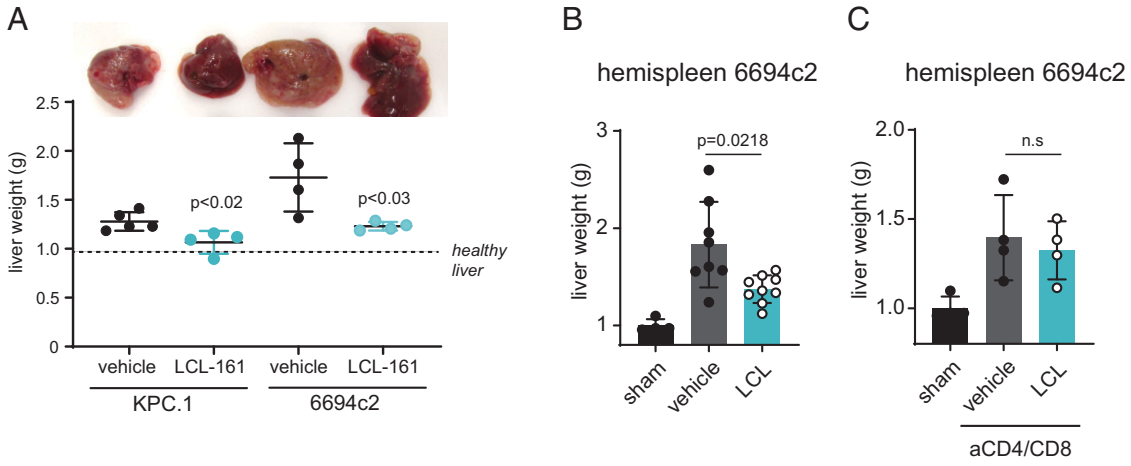

FIGURE 3. cIAP1/2 antagonism induces T cell immunity against PDAC liver metastases. (**A**) KPC cells or 6694c2 cells were seeded into the liver via hemispleen injection. Liver photographs and weights on day 18 are shown. (**B**) 6694c2 cells were seeded into the liver via hemispleen injection. Mice were treated with LCL-161. Liver weights at 18 d postimplantation are shown. (**C**) 6694c2 cells were seeded into the liver via hemispleen injection. Mice were treated with LCL-161 and with isotypes or depleting Abs to CD4/CD8. Liver weights at 18 d postimplantation are shown.

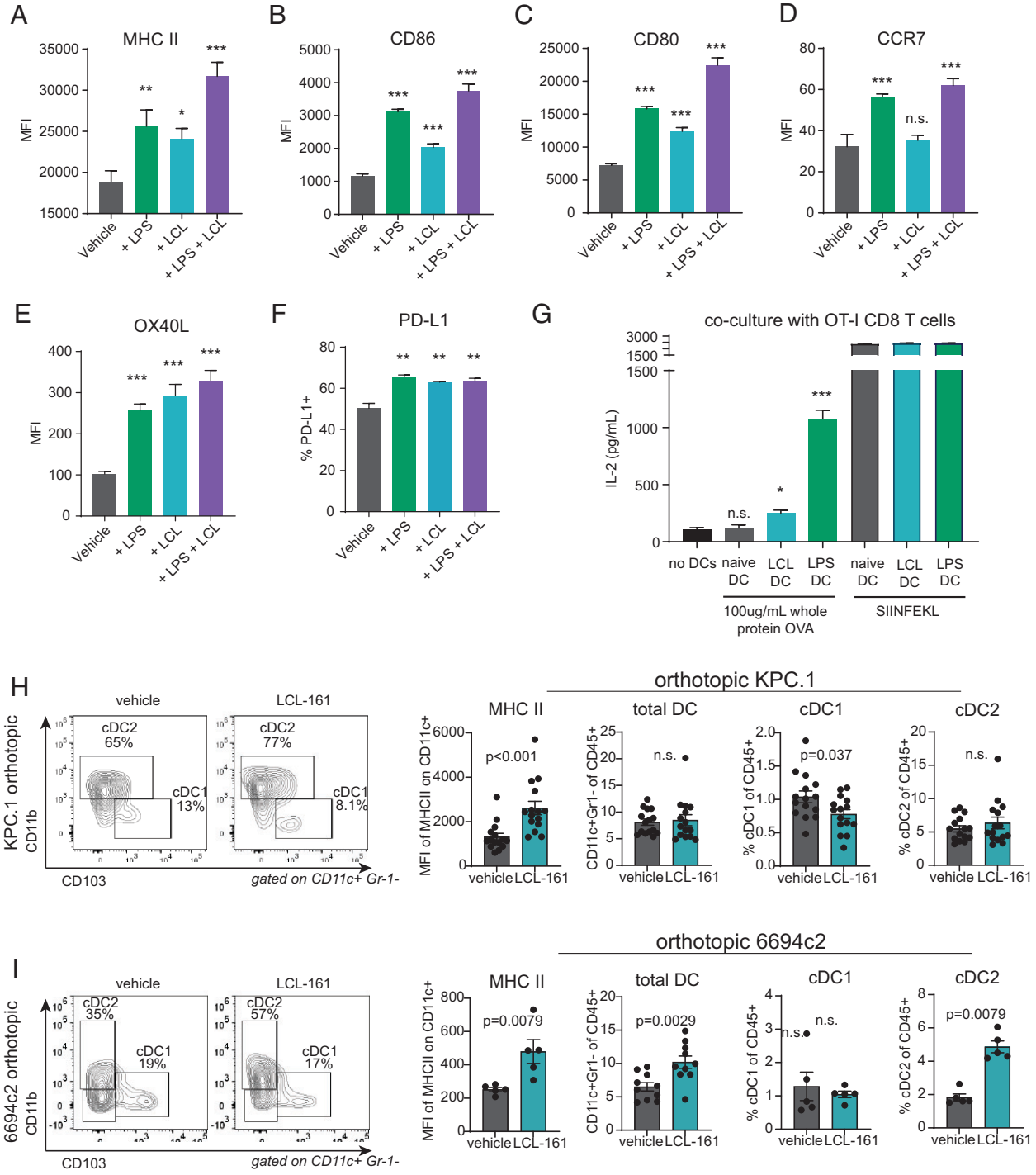

FIGURE 4. DCs are activated by cIAP1/2 antagonism in vitro and in vivo. (**A**–**F**) BMDCs were differentiated using GM-CSF and IL-4 for 7 d, washed, and cultured with media containing vehicle, 500 nM LCL-161, 100 nM LPS, or a combination of LCL-161 and LPS for 24 h. Cells were trypsinized and analyzed by flow cytometry for the indicated markers. Results are representative of three independent experiments. (**G**) BMDCs were prepared as in (A)–(F) and cultured with whole OVA protein (OVA) or 100 nM SIINFEKL peptide. Cells were washed three times prior to transfer to new plastic and coculture with naive OT-I CD8 T cells. T cell activation was assessed by production of IL-2 measured by ELISA of 48 h culture supernatants. ANOVA with multiple comparisons was used for statistical significance. (**H**) C57BL/6 mice were inoculated orthotopically with 50,000 KPC.1 cells suspended in Matrigel and dosed with vehicle or LCL-161 (75 mg/kg) by oral gavage every 3 d starting on day 4. Tumors were harvested 21 d after inoculation and analyzed by flow cytometry. Representative flow plots are gated on $CD45^+Gr\text{-}1^-CD11c^+$ DCs and show gating scheme for cDC1 and cDC2 populations. Mean fluorescence intensity (MFI) of MHC class II on total DCs is quantified. Total DC, cDC1, and cDC2 populations are quantified as percentages of $CD45^+$ singlets. A Mann–Whitney *U* test was used for statistical significance. (**I**) As in (H), but with orthotopic implantation of 6694c2 cells. Error bars are SEM throughout. In (A)–(G), $*p < 0.05$, $**p < 0.01$, $***p < 0.001$.

costimulatory ligands but may have less of an effect on DC trafficking to the draining lymph node.

To assess whether cIAP1/2 antagonism in DCs would be sufficient to induce cross-presentation and activation of naive CD8 T cells, we cultured BMDCs with OVA protein and LCL-161. After washing and replating with OT-I T cells, we observed significant activation of naive CD8 T cells as evidenced by elevated IL-2 production when CD8 T cells were primed by LCL-161–treated DCs cultured with

OVA protein as compared with immature BMDCs exposed to OVA alone. LPS activation and pulsing with SIINFEKL peptide were used as positive controls (Fig. 4G).

We also examined intratumoral DCs from two different orthotopically implanted pancreatic cancer models (Fig. 4H, 4I). Tumor infiltrates were gated on $CD11c^+Gr\text{-}1^-$ DCs and further subgated into $CD103^+$ conventional type 1 DCs (cDC1s) or $CD11b^+$ conventional type 2 DCs (cDC2s). Although modest differences in cDC1 or cDC2 frequencies were observed, no consistent pattern emerged across the models. We did observe a significant increase in MHC class II expression on total DCs from KPC.1 and 6694c2 tumors, suggesting that cIAP1/2 antagonism can contribute to DC activation in vivo (Fig. 4H, 4I).

Pancreatic cancer is highly infiltrated by both granulocytic and monocytic suppressive myeloid cells (35). To test whether alterations in NF-κB signaling had a direct effect on the myeloid cell phenotype, we examined MDSC function in vitro. LCL-161 had no effect on the ability of MDSCs to suppress T cell proliferation (Supplemental Fig. 2A, 2B). We also did not observe changes in the frequency of MDSC populations in tumor infiltrates in vivo from mice bearing orthotopic KPC.1 tumors (Supplemental Fig. 2C).

Live-passage organoid model of poorly immunogenic tumors reveals an orchestrating role for T cells

Most human pancreatic cancers are poorly infiltrated by T cells and have a dense desmoplastic stroma (35). This paucity of T cells may reflect defects in T cell priming. Pancreatic tumors in mice and humans express shared tumor Ags (36, 37), and multiple groups have demonstrated that immune adjuvants such as anti-CD40 or radiation can generate endogenous antitumor immunity targeting tumor Ags in poorly immunogenic pancreatic cancer models (26, 38–40). To better model poorly immunogenic tumors and their stroma in mice, we developed a live-passage organoid-derived model. The murine pancreatic cancer organoid line M8 was implanted orthotopically into C57BL/6 mice (24). Upon establishment of primary tumors, the tumor mass was excised, digested, and the single-cell suspension was mixed with Matrigel and reimplanted orthotopically into new host mice (passage 1). Masson's trichrome staining shows a desmoplastic reaction in M8 organoid–derived tumors that was unaffected by treatment with cIAP1/2 antagonism (Fig. 5A). The M8 line was then continuously maintained as a live-passage model from mouse to mouse for subsequent experiments. M8 tumors are poorly immunogenic in C57BL/6 mice, as evidenced by lack of response to treatment with PD-1 blockade. Nevertheless, treatment with cIAP1/2 antagonism reduced tumor burden by ~50% (Fig. 5B). After initial establishment in mice, the pattern of immune infiltrates was remarkably consistent through passage >20, indicating a reproducible host response to the M8 tumor line (Fig. 5C).

To determine which immune cell types are necessary for cIAP1/2 antagonism in poorly immunogenic pancreatic cancer, we implanted live-passage M8 tumors into mice deficient in selected immune cells. Across our various models tested, B cells were dispensable, but CD8 T cells and $Batf3^+$ DCs were most likely required for the efficacy of cIAP1/2 antagonism in vivo (Fig. 5D), given that therapeutic efficacy was reduced in $B2m^{-/-}$ and $Batf3^{-/-}$ mice. These data are consistent with our previously reported findings in 6694c2 tumors (12). We extended these findings to show that spleens of M8 tumor-bearing mice contained Ag-specific T cells as demonstrated by IFN-γ ELISPOT (Fig. 5E). These T cells were specific to Ags displayed by M8 tumor cells, but not by the closely related cell line 6694c2 (Fig. 5E). Upon examination of the tumor infiltrates from vehicle- or LCL-161–treated M8 orthotopic tumor-bearing mice, we found that the frequency of CD8 and CD4 T cells was low (<2% of total $CD45^+$ cells) and that these frequencies were not increased by LCL-161 (Fig. 5F). These findings of a paucity of T cells were confirmed by immunohistochemistry for CD3, whereby rare T cells could be found around the edges of the tumor mass, but neither the frequency nor the spatial localization was affected by cIAP1/2 antagonism (Fig. 5G). Overall, our results from the M8 model suggested that surprisingly few T cells were required to mediate the antitumor effects observed with cIAP1/2 antagonism.

Live-passage organoid model into $TCR\alpha^{-/-}$ mice allows for homeostatic expansion of tumor-specific T cells

To further investigate a requirement for T cells, we implanted live-passage organoids into $TCR\alpha^{-/-}$ hosts. To our surprise, we observed a reduction in tumor size upon treatment with cIAP1/2 antagonism (Fig. 6A, 6B). We hypothesized that rare T cells contained in the tumor inoculum and transplanted into lymphopenic hosts could undergo homeostatic proliferation and mediate the response to subsequent treatment with LCL-161. Upon treatment of the tumor inoculum with depleting Abs to CD4 and CD8, the therapeutic effect of LCL-161 was ablated, confirming that T cells in the live-passage inoculum were responsible for tumor control (Fig. 6B). Given that all of these T cells were derived from clonotypes that had infiltrated pancreatic tumors, this model afforded an opportunity to evaluate the effects of cIAP1/2 antagonism in vivo in tumor-responding T cells. We used FACS to isolate the CD4 and CD8 T cells out of spleens or tumors of M8 tumor-bearing $TCR\alpha^{-/-}$ mice to enrich for αβ T cells that originated from the initial endogenous T cell response to M8 tumors in immune-competent animals. We then performed limited bulk RNA sequencing and asked which genes were differentially expressed in tumor-infiltrating CD8 T cells treated with LCL-161 as compared with vehicle (Fig. 6C). The top upregulated gene was 4-1BB (*Tnfrsf9*), a known costimulatory receptor upregulated on recently activated T cells. Serpin proteases were also upregulated, including *Serpinb9*, which protects granzyme-secreting cytolytic cells from fratricide (41). Intriguingly, the top downregulated gene was *Vsir* encoding the negative regulatory receptor VISTA. Gene set enrichment analysis for both CD4 and CD8 T cells showed increased cell cycle–related transcripts and increased NF-κB target genes (Fig. 6D). Increased cell cycle was unexpected give our inability to show increased frequencies of intratumoral T cells, although proliferation may be counterbalanced by other factors such as increased rates of apoptosis or exit from the tumor. Comparison of differentially expressed genes overlapping between spleen and tumor also revealed a signature of cIAP1/2 antagonism on T cells consistent with increased NF-κB activation (Supplemental Fig. 3). Thus, we postulate that both CD4 and CD8 T cells in vivo are direct cellular targets of cIAP1/2 antagonism, displaying hallmarks of increased NF-κB2 signaling consistent with loss of cIAP1/2.

cIAP1/2 antagonism combines with adoptive transfer of Ag-specific T cells

To test whether cIAP1/2 antagonism could be combined with adoptive transfer of known Ag-specific T cells, we used a model of CD8 T cells recognizing the self-antigen TRP1 expressed by melanocytes and overexpressed in melanoma. We had previously cloned mice by somatic cell nuclear transfer from the nuclei of CD8 T cells recognizing TRP1 presented by $H\text{-}2D^b$ with physiologic affinity (21, 23). Adoptive transfer of naive $TRP1^{high}$ CD8 T cells has very modest activity against B16 melanoma, which provides an opportune platform for evaluation of combination therapies aimed at augmenting CD8 T cell priming or function (21). LCL-161 significantly delayed growth of B16 melanoma in wild-type, but not $TCR\alpha^{-/-}$, hosts, indicating T cell dependency of cIAP1/2 antagonism in melanoma (Fig. 7A). Mice bearing B16 melanoma were then treated with adoptive transfer of $TRP1^{high}$ CD8 T cells, LCL-161, or the combination.

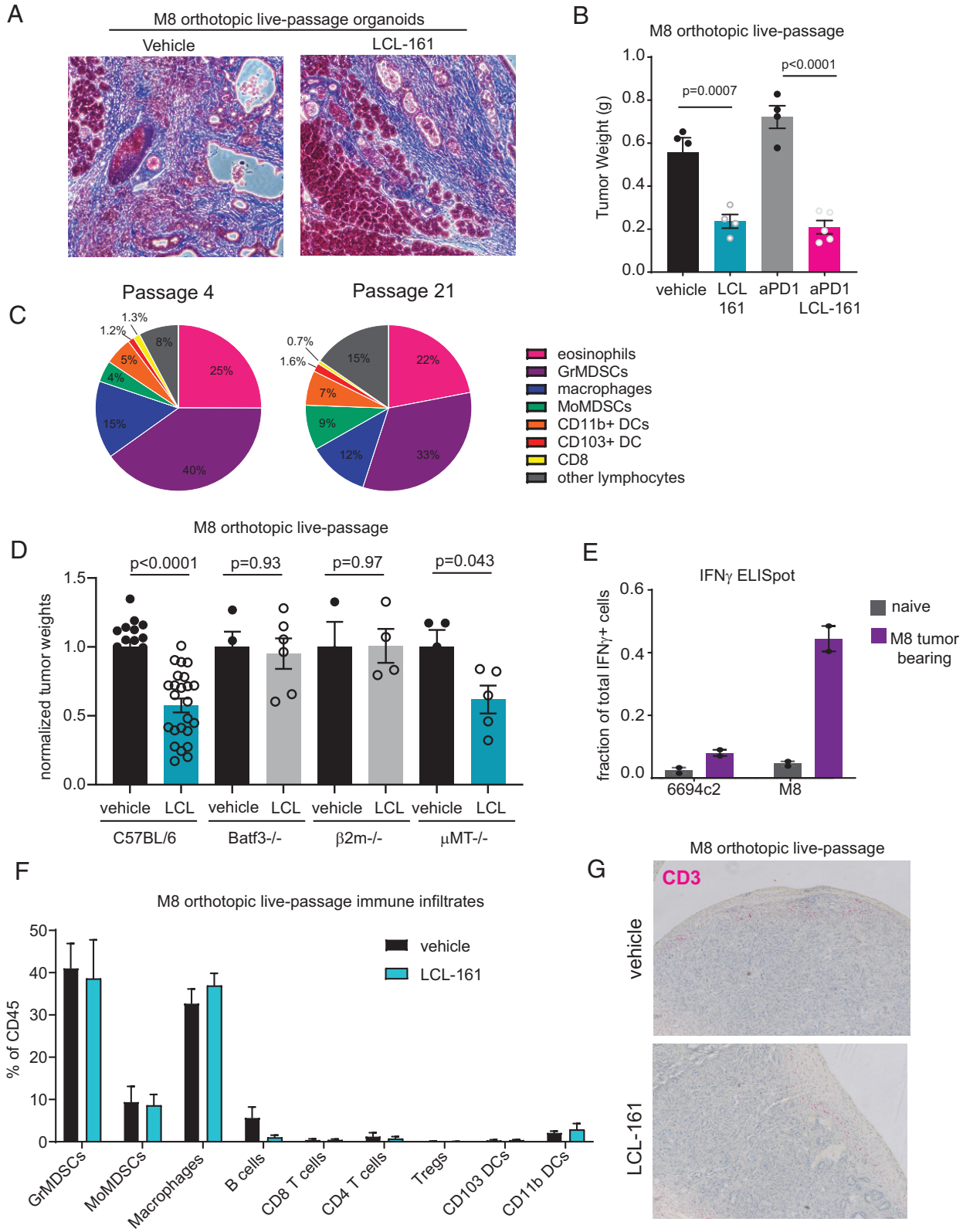

FIGURE 5. Live-passage organoid model contains few T cells but responds to cIAP1/2 antagonism in a T cell–dependent manner. (**A**) M8 live-passage organoid tumors grown orthotopically in C57BL/6 mice were analyzed by Masson's trichrome staining. Original magnification ×20. (**B**) C57BL/6 mice were implanted orthotopically with M8 live-passage organoids and treated with vehicle or LCL-161 (75 mg/kg) by oral gavage and isotype or anti–PD-1 Abs (150 μg/mouse) every 3 d starting on day 4. Tumors were harvested on day 21. Results are representative of three independent experiments. (**C**) At passage 4 or passage 21, orthotopically implanted M8 live-passage organoid tumors were harvested at day 18 from mice treated with vehicle, digested, and analyzed by flow cytometry. Cell types were gated from $CD45^+$ cells and are defined as follows: eosinophils ($CD11b^+Gr1^-Siglec\ F^+$), granulocytic (Gr)MDSCs ($CD11b^+Gr1^{high}$), macrophages ($CD11b^+Gr1^-CD11c^-$), monocytic (Mo)MDSCs ($CD11b^+Gr1^{mid}$), $CD11b^+$ DCs ($CD11b^+Gr1^-Siglec\ F^-CD11c^+I\text{-}A^{b+}$), $CD103^+$ DCs ($CD11b^-Gr1^-CD11c^+Ly6c^-Siglec\ F^-CD103^+$), CD8 T cells ($CD11b^-CD8\alpha^+$), and other lymphocytes ($SSC^{low}CD11b^-CD8\alpha^-$). (**D**) C57BL/6, $Batf3^{-/-}$, $\beta2m^{-/-}$, or $\mu MT^{-/-}$ mice were implanted orthotopically with M8 live-passage organoids and treated with vehicle or LCL-161 (75 mg/kg) by oral gavage every 3 d starting on day 4. Tumors were harvested on day 21. Tumor weights were normalized to the average of the vehicle control mice, and results *(Figure legend continues)*

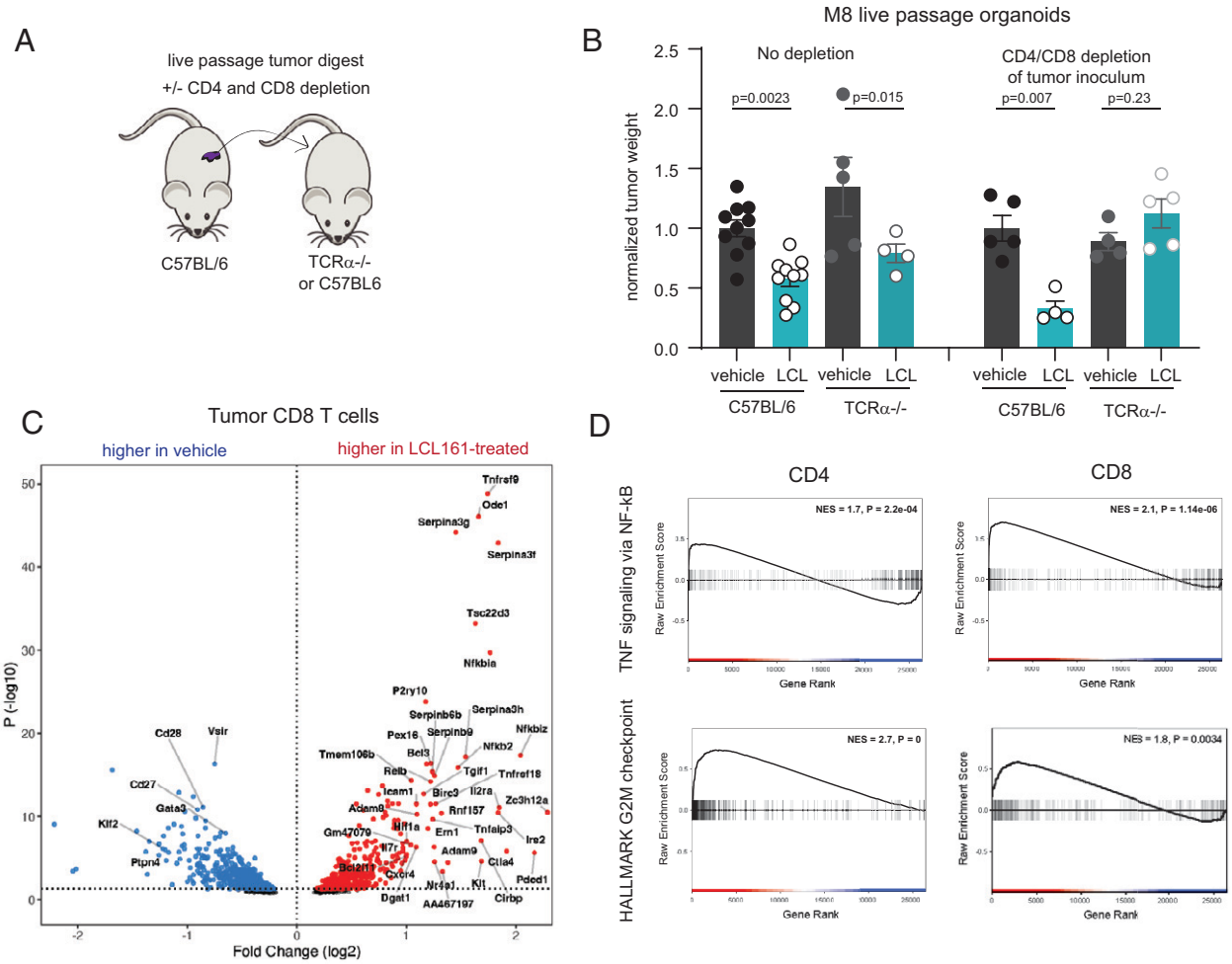

FIGURE 6. T cells transferred with the M8 live-passage inoculum expand in lymphopenic hosts and reveal a profile of direct cIAP1/2 antagonism. (**A**) Experimental diagram showing use of depleting Abs in the tumor inoculum. (**B**) C57BL/6 or TCRα$^{-/-}$ mice were implanted orthotopically with M8 live-passage organoids and treated with vehicle or LCL-161 (75 mg/kg) by oral gavage every 3 d starting on day 4. Tumors were harvested on day 21. Tumor weights were normalized to the average of the vehicle control mice, and results shown are pooled from two experiments. In the left panels, the inoculum was untreated; in the right panels, the inoculum was treated with 10 μg/ml anti-CD4 and anti-CD8 depleting Abs prior to inoculation. Error bars are SEM. ANOVA with multiple comparisons was used. n = 4–10 mice per group. (**C** and **D**) TCRα$^{-/-}$ mice were implanted orthotopically with M8 live-passage organoids and treated with vehicle or LCL-161 (75 mg/kg) by oral gavage every 3 d starting on day 4. Tumors and spleens were harvested on day 12 after three doses of LCL-161 and single-cell suspensions were prepared. CD4 and CD8 T cells were isolated by FACS and subjected to limited bulk transcriptional profiling. n = 3 per group. (C) Differential gene expression analysis comparing CD8 T cells from tumors treated with vehicle or LCL-161. (D) Gene set enrichment analysis for hallmark TNFA signaling via NF-κB and hallmark G2M checkpoint gene sets was performed on tumor-infiltrating CD4 and CD8 T cell datasets.

Combination therapy was more effective at delaying tumor growth than either single agent alone (Fig. 7B).

To use our TRP1 mice in a model of pancreatic cancer, we cloned the gene expressing TRP1 into the 6694c2 pancreatic tumor cell line to generate C2VTrp1 cells. Mice were inoculated s.c. with C2VTrp1 cells and tumor growth was monitored over time. Adoptive transfer of naive TRP1^{high} CD8 T cells alone had a negligible effect in this setting. Treatment with LCL-161 significantly reduced tumor growth but was more effective when combined with adoptive transfer of TRP1^{high} CD8 T cells (Fig. 7C). Furthermore, we examined circulating CD8 T cells from mice at day 14 after tumor inoculation (after three treatments of LCL-161) and observed increased expression of the activation marker CD44 on transferred TRP1^{high} CD8 T cells (Supplemental Fig. 4A–C), demonstrating increased activation of

shown are pooled from multiple experiments. (**E**) Splenocytes of C57BL/6 naive mice or mice bearing M8 live-passage organoid tumor were plated with the pancreatic cancer cell line 6694c2 or M8 organoid-derived cells that had been adapted to flat culture conditions. In separate wells, splenocytes were cultured with anti-CD3/CD28 beads to determine the maximum number of IFN-γ–producing cells. Cells were analyzed by ELISPOT, and values shown are normalized to the number of spots obtained in the anti-CD3/CD28 wells. (**F**) Orthotopically implanted M8 live-passage organoid tumors were harvested at day 18 from mice treated with vehicle or LCL-161, digested, and analyzed by flow cytometry. Cell types were gated from CD45$^+$ cells and are defined as follows: GrMDSCs (CD11b$^+$Gr1$^+$Ly6C$^-$CX3CR1$^-$), MoMDSCs (CD11b$^+$Gr1$^+$Ly6C$^{+/-}$CX3CR1$^{+/-}$), macrophages (CD11b$^+$Gr1$^-$CD11c$^-$), B cells (CD11b$^-$Gr1$^-$B220$^+$), CD8 T cells (CD11b$^-$CD8α$^+$), CD4 T cells (CD11b$^-$CD4$^+$Foxp3$^-$), regulatory T cells (Tregs; CD11b$^-$CD4$^+$Foxp3$^+$), CD103$^+$ DCs (CD11b$^-$Gr1$^-$CD11c$^+$Ly6c$^-$Siglec F$^-$CD103$^+$), and CD11b$^+$ DCs (CD11b$^+$Gr1$^-$CD11c$^+$). No significant differences were observed between vehicle and LCL-161 treatment groups. Results are representative of five independent experiments. (**G**) Tumors from mice treated as in (E) were formalin fixed and paraffin embedded and analyzed by immunohistochemistry for CD3 (pink). Original magnification ×10 Error bars are SEM throughout. ANOVA with multiple comparisons was used throughout.

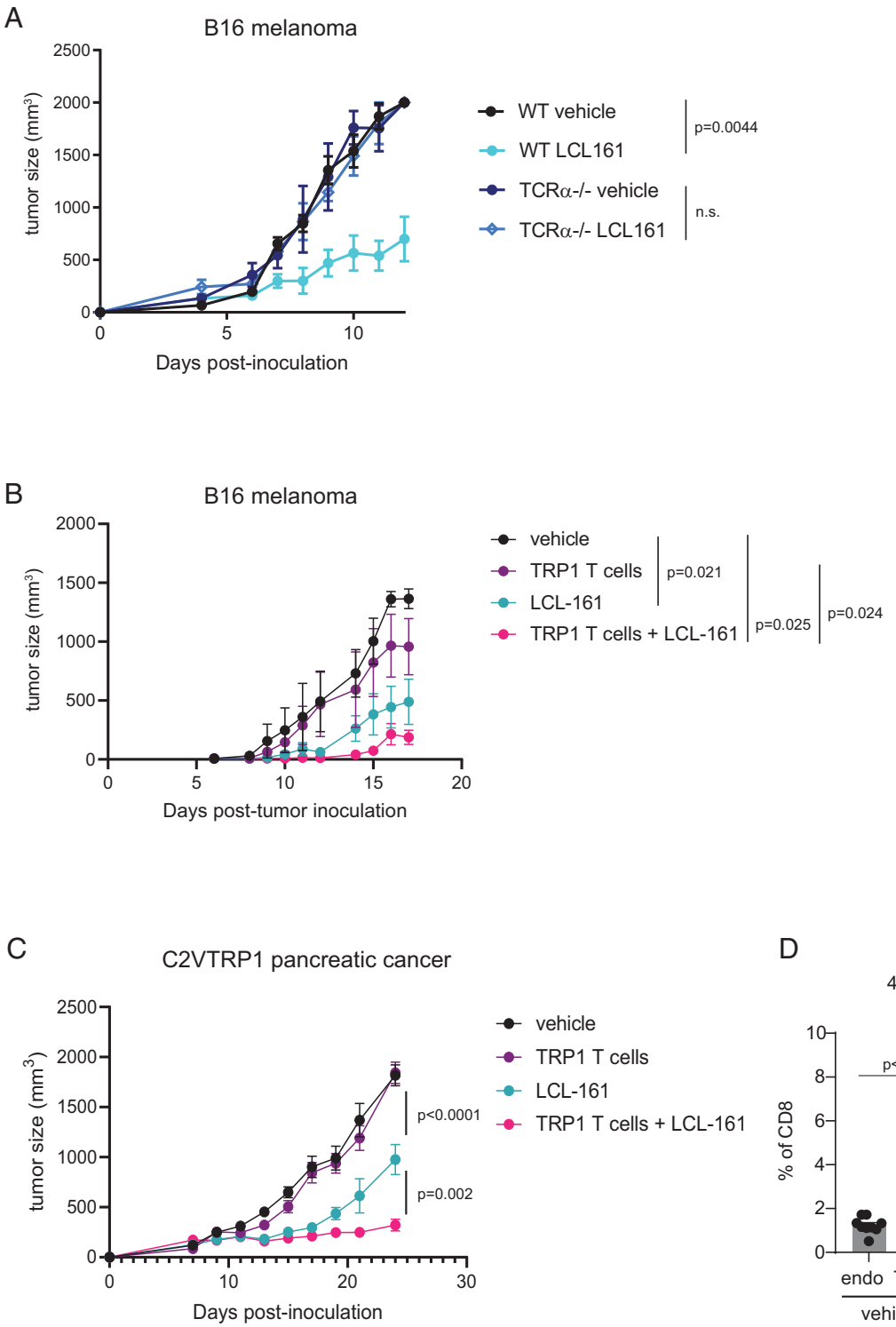

FIGURE 7. cIAP1/2 antagonism combines with adoptive T cell therapy and induces 4-1BB expression in vivo. (**A**) B16-OVA cells (2×10^6) were implanted s.c. in C57BL/6 mice or TCR$\alpha^{-/-}$ mice. Mice were dosed with 75 mg/kg LCL-161 by oral gavage every 3 d starting on day 1 postimplantation. Tumor volumes were measured by precision calipers. (**B**) CD8 T cells were isolated from a TRP1^{high} mouse and activated in vitro for 48 h with anti-CD3/CD28 and vehicle or 500 nM LCL-161. CD8 T cells were washed and adoptively transferred into C57BL/6 mice that had been s.c. inoculated with 250,000 B16-F10 melanoma cells 5 d prior to T cell transfer. Mice were also treated with vehicle or LCL-161 (75 mg/kg) by oral gavage every 3 d starting on day 5. $n = 5$ per group. Vehicle, no T cells, vehicle oral gavage; TRP1 T cells, vehicle-treated TRP1 cells, vehicle oral gavage; LCL-161, no T cells, LCL-161 oral gavage; TRP1 T cells + LCL-161, LCL-161 treated TRP1 cells, LCL-161 oral gavage. (**C**) C57BL/6 mice were inoculated s.c. with 300,000 C2VTRP1 cells. On day 7, some mice received adoptive transfer of naive TRP1^{high};CD45.1^{+} CD8 T cells as indicated. Mice were also treated with vehicle or 75 mg/kg LCL-161 by oral gavage every 2 d starting on day 7. Tumor volumes were measured over time. (**D**) Flow cytometry analysis of 4-1BB expression on activated peripheral blood CD8 T cells from mice in (C). Gating strategy is shown in Supplemental Fig. 4. Endo, endogenous T cells (CD45.1^{-}). Error bars are SEM throughout.

tumor-specific T cells in vivo. By day 17, peripheral TRP1 as well as endogenous CD8 and CD4 T cells displayed increased expression of CD44 (Supplemental Fig. 4D, 4E). We further examined expression of 4-1BB, the gene most significantly upregulated by cIAP1/2 antagonism from our transcriptional profiling (Fig. 6C). 4-1BB was weakly detected on CD4 T cells and $CD44^{low}$ naive T cells (Supplemental Fig. 4A, 4B). Within $CD44^{high}$ activated T cells, we observed higher frequencies of 4-1BB^{+} TRP1 and endogenous CD8 T cells in mice treated with LCL-161 (Fig. 4D), indicating qualitative enhancement in activation of tumor-specific CD8 T cells.

Discussion

We and others have previously reported a variety of beneficial effects of cIAP1/2 antagonism on immune cells (1, 8–12). These agents mimic costimulation in T cells, thereby increasing proliferation and cytokine production from CD4, CD8, and invariant NKT cells (8, 11). NK cell production of GM-CSF is also augmented by cIAP1/2 antagonism. DCs produce more IL-12, express higher levels of costimulatory ligands, and are better at presenting Ag to naive T cells (8). Macrophages become reprogrammed by cIAP1/2 antagonism to phagocytose live tumor cells, an effect that is greatly augmented by increased T cell production of cytokines such as IFN-γ and lymphotoxin (12, 18). Oncolytic virotherapy is improved by cIAP1/2 antagonism (42–44), and both T cell and chimeric Ag receptor (CAR) T cell ability to kill tumor cells via TNF-α is boosted by cIAP1/2 antagonism across a variety of difficult-to-treat tumor types (17, 45–47). cIAP1/2 antagonism is thus a potent strategy for inducing antitumor immunity against a wide range of tumors, including notoriously refractory cancers such as pancreatic cancer or cancers that have lost expression of MHC class I (12).

We have clarified several key points that add to this growing body of data supporting induction of antitumor immunity by cIAP1/2 antagonists. First, the Ag-specific nature of T cells augmented by cIAP1/2 antagonism had not formally been demonstrated, and in this study we show evidence for Ag specificity via multiple approaches: induction of immunologic memory, quantification of tumor-specific T cells by IFN-γ ELISPOT, and the use of adoptively transferred tumor-specific CD8 T cells. Second, the profound ability of rare T cells to induce tumor regression was observed, but not fully explored other than to identify lymphotoxin as the likely key factor required for cross-activation of phagocidal macrophages (12). In this study, we provide full transcriptional profiling from ex vivo–isolated CD4 and CD8 T cells using a unique live-passage organoid model into $TCR\alpha^{-/-}$ hosts that allows for expansion and enrichment of tumor-specific T cells. We identified several potential pathways by which cIAP1/2 antagonism might mechanistically enhance T cell activity, including upregulation of 4-1BB, downregulation of VISTA, or expression of serpin proteases to protect against granzyme-mediated cell death. These pathways are worth further exploration as inspiration for combination therapy. Third, although cIAP1/2 are expressed in nearly all immune cells, we identified an encouraging lack of effect of cIAP1/2 antagonism on granulocytic and monocytic MDSCs, cell types that had not previously been examined.

Pancreatic cancer in humans contains a range of T cell infiltrates, although responses to checkpoint blockade have been universally poor outside of the rare microsatellite instability–high subset (48). We hypothesize that failure of immunotherapy in pancreatic cancer and other poorly responsive tumor types is in part due to inadequate T cell priming. In this study, we have shown that cIAP1/2 antagonism has pleiotropic beneficial effects on antitumor immunity, including increased activation of DCs and direct effects on tumor-specific T cells leading to overall increased activation, increased control of tumor growth in vivo, synergy with multiple immunotherapy modalities, and immunologic memory. Furthermore, we confirm our previous findings that even poorly immunogenic tumors with a paucity of T cells can experience T cell–dependent antitumor immunity, and we provide transcriptional clues into how these rare T cells coordinate downstream immune responses.

Acknowledgments

We thank Scott Gerber and David Linehan for hemispleen injection training.

Disclosures

S.K.D. received research funding for this project from Novartis Institute for Biomedical Research. K.R., J.J.A., and M.P. are employees of Novartis Institute for Biomedical Research. S.K.D. received research funding unrelated to this project from Eli Lilly and Company, Genocea Biosciences, and Bristol Myers Squibb and is a founder, science advisory board member, and equity holder in Kojin. M.D. has research funding unrelated to this project from Novartis and Eli Lilly; he has received consulting fees from Tillotts Pharma, ORIC Pharmaceuticals, Partner Therapeutics, SQZ Biotech, AzurRx, Eli Lilly, Mallinckrodt Pharmaceuticals, Aditum, Foghorn Therapeutics, and Moderna, and he is a member of the scientific advisory board for Neoleukin Therapeutics. The other authors have no financial conflicts of interest.

References

1. Kocab, A. J., and C. S. Duckett. 2016. Inhibitor of apoptosis proteins as intracellular signaling intermediates. *FEBS J.* 283: 221–231.
2. Gaither, A., D. Porter, Y. Yao, J. Borawski, G. Yang, J. Donovan, D. Sage, J. Slisz, M. Tran, C. Straub, et al. 2007. A Smac mimetic rescue screen reveals roles for inhibitor of apoptosis proteins in tumor necrosis factor-α signaling. *Cancer Res.* 67: 11493–11498.
3. Petersen, S. L., L. Wang, A. Yalcin-Chin, L. Li, M. Peyton, J. Minna, P. Harran, and X. Wang. 2007. Autocrine TNFα signaling renders human cancer cells susceptible to Smac-mimetic-induced apoptosis. *Cancer Cell* 12: 445–456.
4. Varfolomeev, E., J. W. Blankenship, S. M. Wayson, A. V. Fedorova, N. Kayagaki, P. Garg, K. Zobel, J. N. Dynek, L. O. Elliott, H. J. Wallweber, et al. 2007. IAP antagonists induce autoubiquitination of c-IAPs, NF-κB activation, and TNFα-dependent apoptosis. *Cell* 131: 669–681.
5. Vince, J. E., W. W. Wong, N. Khan, R. Feltham, D. Chau, A. U. Ahmed, C. A. Benetatos, S. K. Chunduru, S. M. Condon, M. McKinlay, et al. 2007. IAP antagonists target cIAP1 to induce TNFα-dependent apoptosis. *Cell* 131: 682–693.
6. Varfolomeev, E., T. Goncharov, A. V. Fedorova, J. N. Dynek, K. Zobel, K. Deshayes, W. J. Fairbrother, and D. Vucic. 2008. c-IAP1 and c-IAP2 are critical mediators of tumor necrosis factor α (TNFα)-induced NF-κB activation. *J. Biol. Chem.* 283: 24295–24299.
7. Dueber, E. C., A. J. Schoeffler, A. Lingel, J. M. Elliott, A. V. Fedorova, A. M. Giannetti, K. Zobel, B. Maurer, E. Varfolomeev, P. Wu, et al. 2011. Antagonists induce a conformational change in cIAP1 that promotes autoubiquitination. *Science* 334: 376–380.
8. Dougan, M., S. Dougan, J. Slisz, B. Firestone, M. Vanneman, D. Draganov, G. Goyal, W. Li, D. Neuberg, R. Blumberg, et al. 2010. IAP inhibitors enhance co-stimulation to promote tumor immunity. *J. Exp. Med.* 207: 2195–2206.
9. Matsuzawa, A., P. H. Tseng, S. Vallabhapurapu, J. L. Luo, W. Zhang, H. Wang, D. A. Vignali, E. Gallagher, and M. Karin. 2008. Essential cytoplasmic translocation of a cytokine receptor-assembled signaling complex. *Science* 321: 663–668.
10. Zarnegar, B. J., Y. Wang, D. J. Mahoney, P. W. Dempsey, H. H. Cheung, J. He, T. Shiba, X. Yang, W. C. Yeh, T. W. Mak, et al. 2008. Noncanonical NF-κB activation requires coordinated assembly of a regulatory complex of the adaptors cIAP1, cIAP2, TRAF2 and TRAF3 and the kinase NIK. *Nat. Immunol.* 9: 1371–1378.
11. Clancy-Thompson, E., L. Ali, P. T. Bruck, M. A. Exley, R. S. Blumberg, G. Dranoff, M. Dougan, and S. K. Dougan. 2018. IAP antagonists enhance cytokine production from mouse and human iNKT cells. *Cancer Immunol. Res.* 6: 25–35.
12. Roehle, K., L. Qiang, K. S. Ventre, D. Heid, L. R. Ali, P. Lenehan, M. Heckler, S. J. Crowley, C. T. Stump, G. Ro, et al. 2021. cIAP1/2 antagonism eliminates MHC class I-negative tumors through T cell-dependent reprogramming of mononuclear phagocytes. *Sci. Transl. Med.* 13: eabf5058.
13. Dougan, S. K., and M. Dougan. 2018. Regulation of innate and adaptive antitumor immunity by IAP antagonists. *Immunotherapy* 10: 787–796.
14. Gentle, I. E., I. Moelter, N. Lechler, S. Bambach, S. Vucikuja, G. Häcker, and P. Aichele. 2014. Inhibitors of apoptosis proteins (IAPs) are required for effective T-cell expansion/survival during antiviral immunity in mice. *Blood* 123: 659–668.
15. Giardino Torchia, M. L., I. Munitic, E. Castro, J. Herz, D. B. McGavern, and J. D. Ashwell. 2015. c-IAP ubiquitin protein ligase activity is required for 4-1BB signaling and $CD8^{+}$ memory T-cell survival. *Eur. J. Immunol.* 45: 2672–2682.
16. Knights, A. J., J. Fucikova, A. Pasam, S. Koernig, and J. Cebon. 2013. Inhibitor of apoptosis protein (IAP) antagonists demonstrate divergent immunomodulatory properties in human immune subsets with implications for combination therapy. *Cancer Immunol. Immunother.* 62: 321–335.

17. Beug, S. T., C. E. Beauregard, C. Healy, T. Sanda, M. St-Jean, J. Chabot, D. E. Walker, A. Mohan, N. Earl, X. Lun, et al. 2017. Smac mimetics synergize with immune checkpoint inhibitors to promote tumour immunity against glioblastoma. [Published erratum appears in 2018 *Nat. Commun.* 9: 16231.] *Nat. Commun.* 8: 14278.
18. Chesi, M., N. N. Mirza, V. M. Garbitt, M. E. Sharik, A. C. Dueck, Y. W. Asmann, I. Akhmetzyanova, H. E. Kosiorek, A. Calcinotto, D. L. Riggs, et al. 2016. IAP antagonists induce anti-tumor immunity in multiple myeloma. *Nat. Med.* 22: 1411–1420.
19. Crowley, S. J., P. T. Bruck, M. A. Bhuiyan, A. Mitchell-Gears, M. J. Walsh, K. Zhangxu, L. R. Ali, H. J. Jeong, J. R. Ingram, D. M. Knipe, et al. 2020. Neoleukin-2 enhances anti-tumour immunity downstream of peptide vaccination targeted by an anti-MHC class II VHH. *Open Biol.* 10: 190235.
20. Li, J., K. T. Byrne, F. Yan, T. Yamazoe, Z. Chen, T. Baslan, L. P. Richman, J. H. Lin, Y. H. Sun, A. J. Rech, et al. 2018. Tumor cell-intrinsic factors underlie heterogeneity of immune cell infiltration and response to immunotherapy. *Immunity* 49: 178–193.e7.
21. Dougan, S. K., M. Dougan, J. Kim, J. A. Turner, S. Ogata, H. I. Cho, R. Jaenisch, E. Celis, and H. L. Ploegh. 2013. Transnuclear TRP1-specific CD8 T cells with high or low affinity TCRs show equivalent antitumor activity. *Cancer Immunol. Res.* 1: 99–111.
22. Manguso, R. T., H. W. Pope, M. D. Zimmer, F. D. Brown, K. B. Yates, B. C. Miller, N. B. Collins, K. Bi, M. W. LaFleur, V. R. Juneja, et al. 2017. In vivo CRISPR screening identifies *Ptpn2* as a cancer immunotherapy target. *Nature* 547: 413–418.
23. Clancy-Thompson, E., C. A. Devlin, P. M. Tyler, M. M. Servos, L. R. Ali, K. S. Ventre, M. A. Bhuiyan, P. T. Bruck, M. E. Birnbaum, and S. K. Dougan. 2018. Altered binding of tumor antigenic peptides to MHC class I affects $CD8^+$ T cell-effector responses. *Cancer Immunol. Res.* 6: 1524–1536.
24. Boj, S. F., C. I. Hwang, L. A. Baker, I. I. Chio, D. D. Engle, V. Corbo, M. Jager, M. Ponz-Sarvise, H. Tiriac, M. S. Spector, et al. 2015. Organoid models of human and mouse ductal pancreatic cancer. *Cell* 160: 324–338.
25. Soares, K. C., K. Foley, K. Olino, A. Leubner, S. C. Mayo, A. Jain, E. Jaffee, R. D. Schulick, K. Yoshimura, B. Edil, and L. Zheng. 2014. A preclinical murine model of hepatic metastases. *J. Vis. Exp.* (91): 51677.
26. Stump, C. T., K. Roehle, N. Manjarrez Orduno, and S. K. Dougan. 2021. Radiation combines with immune checkpoint blockade to enhance T cell priming in a murine model of poorly immunogenic pancreatic cancer. *Open Biol.* 11: 210245.
27. Lenehan, P. J., A. Cirella, A. M. Uchida, S. J. Crowley, T. Sharova, G. Boland, M. Dougan, S. K. Dougan, and M. Heckler. 2021. Type 2 immunity is maintained during cancer-associated adipose tissue wasting. *Immunother. Adv.* 1: ltab011.
28. Dougan, M., G. Dranoff, and S. K. Dougan. 2019. GM-CSF, IL-3, and IL-5 family of cytokines: regulators of inflammation. *Immunity* 50: 796–811.
29. Le, D. T., E. Lutz, J. N. Uram, E. A. Sugar, B. Onners, S. Solt, L. Zheng, L. A. Diaz, Jr., R. C. Donehower, E. M. Jaffee, and D. A. Laheru. 2013. Evaluation of ipilimumab in combination with allogeneic pancreatic tumor cells transfected with a GM-CSF gene in previously treated pancreatic cancer. *J. Immunother.* 36: 382–389.
30. Dranoff, G., E. Jaffee, A. Lazenby, P. Golumbek, H. Levitsky, K. Brose, V. Jackson, H. Hamada, D. Pardoll, and R. C. Mulligan. 1993. Vaccination with irradiated tumor cells engineered to secrete murine granulocyte-macrophage colony-stimulating factor stimulates potent, specific, and long-lasting anti-tumor immunity. *Proc. Natl. Acad. Sci. USA* 90: 3539–3543.
31. Bayne, L. J., G. L. Beatty, N. Jhala, C. E. Clark, A. D. Rhim, B. Z. Stanger, and R. H. Vonderheide. 2012. Tumor-derived granulocyte-macrophage colony-stimulating factor regulates myeloid inflammation and T cell immunity in pancreatic cancer. *Cancer Cell* 21: 822–835.
32. Pylayeva-Gupta, Y., K. E. Lee, C. H. Hajdu, G. Miller, and D. Bar-Sagi. 2012. Oncogenic Kras-induced GM-CSF production promotes the development of pancreatic neoplasia. *Cancer Cell* 21: 836–847.
33. Waghray, M., M. Yalamanchili, M. Dziubinski, M. Zeinali, M. Erkkinen, H. Yang, K. A. Schradle, S. Urs, M. Pasca Di Magliano, T. H. Welling, et al. 2016. GM-CSF mediates mesenchymal-epithelial cross-talk in pancreatic cancer. *Cancer Discov.* 6: 886–899.
34. Lübbers, J., R. J. Eveline Li, F. S. Gorki, S. C. M. Bruijns, A. Gallagher, H. Kalay, M. Ambrosini, D. Molenaar, J. Van den Bossche, S. J. van Vliet, and Y. van Kooyk. 2021. α2-3 Sialic acid binding and uptake by human monocyte-derived dendritic cells alters metabolism and cytokine release and initiates tolerizing T cell programming. *Immunother. Adv.* 1: ltab012.
35. Balachandran, V. P., G. L. Beatty, and S. K. Dougan. 2019. Broadening the impact of immunotherapy to pancreatic cancer: challenges and opportunities. *Gastroenterology* 156: 2056–2072.
36. Feig, C., J. O. Jones, M. Kraman, R. J. Wells, A. Deonarine, D. S. Chan, C. M. Connell, E. W. Roberts, Q. Zhao, O. L. Caballero, et al. 2013. Targeting CXCL12 from FAP-expressing carcinoma-associated fibroblasts synergizes with anti-PD-L1 immunotherapy in pancreatic cancer. *Proc. Natl. Acad. Sci. USA* 110: 20212–20217.
37. Le, D. T., A. Wang-Gillam, V. Picozzi, T. F. Greten, T. Crocenzi, G. Springett, M. Morse, H. Zeh, D. Cohen, R. L. Fine, et al. 2015. Safety and survival with GVAX pancreas prime and *Listeria monocytogenes*-expressing mesothelin (CRS-207) boost vaccines for metastatic pancreatic cancer. *J. Clin. Oncol.* 33: 1325–1333.
38. Ma, H. S., B. Poudel, E. R. Torres, J. W. Sidhom, T. M. Robinson, B. Christmas, B. Scott, K. Cruz, S. Woolman, V. Z. Wall, et al. 2019. A CD40 agonist and PD-1 antagonist antibody reprogram the microenvironment of nonimmunogenic tumors to allow T-cell-mediated anticancer activity. *Cancer Immunol. Res.* 7: 428–442.
39. Rech, A. J., H. Dada, J. J. Kotzin, J. Henao-Mejia, A. J. Minn, C. Twyman-Saint Victor, and R. H. Vonderheide. 2018. Radiotherapy and CD40 activation separately augment immunity to checkpoint blockade in cancer. *Cancer Res.* 78: 4282–4291.
40. Yasmin-Karim, S., P. T. Bruck, M. Moreau, S. Kunjachan, G. Z. Chen, R. Kumar, S. Grabow, S. K. Dougan, and W. Ngwa. 2018. Radiation and local anti-CD40 generate an effective in situ vaccine in preclinical models of pancreatic cancer. *Front. Immunol.* 9: 2030.
41. Hirst, C. E., M. S. Buzza, C. H. Bird, H. S. Warren, P. U. Cameron, M. Zhang, P. G. Ashton-Rickardt, and P. I. Bird. 2003. The intracellular granzyme B inhibitor, proteinase inhibitor 9, is up-regulated during accessory cell maturation and effector cell degranulation, and its overexpression enhances CTL potency. *J. Immunol.* 170: 805–815.
42. Kim, D. S., H. Dastidar, C. Zhang, F. J. Zemp, K. Lau, M. Ernst, A. Rakic, S. Sikdar, J. Rajwani, V. Naumenko, et al. 2017. Smac mimetics and oncolytic viruses synergize in driving anticancer T-cell responses through complementary mechanisms. [Published erratum appears in 2018 *Nat. Commun.* 9: 2109.] *Nat. Commun.* 8: 344.
43. Cai, J., Y. Lin, H. Zhang, J. Liang, Y. Tan, W. K. Cavenee, and G. Yan. 2017. Selective replication of oncolytic virus M1 results in a bystander killing effect that is potentiated by Smac mimetics. *Proc. Natl. Acad. Sci. USA* 114: 6812–6817.
44. Beug, S. T., S. J. Pichette, M. St-Jean, J. Holbrook, D. E. Walker, E. C. LaCasse, and R. G. Korneluk. 2018. Combination of IAP antagonists and TNF-α-armed oncolytic viruses induce tumor vascular shutdown and tumor regression. *Mol. Ther. Oncolytics* 10: 28–39.
45. Michie, J., P. A. Beavis, A. J. Freeman, S. J. Vervoort, K. M. Ramsbottom, V. Narasimhan, E. J. Lelliott, N. Lalaoui, R. G. Ramsay, R. W. Johnstone, et al. 2019. Antagonism of IAPs enhances CAR T-cell efficacy. *Cancer Immunol. Res.* 7: 183–192.
46. Mo, X., C. Tang, Q. Niu, T. Ma, Y. Du, and H. Fu. 2019. HTiP: high-throughput immunomodulator phenotypic screening platform to reveal IAP antagonists as anti-cancer immune enhancers. *Cell Chem. Biol.* 26: 331–339.e3.
47. Xiao, R., C. T. Allen, L. Tran, P. Patel, S. J. Park, Z. Chen, C. Van Waes, and N. C. Schmitt. 2018. Antagonist of cIAP1/2 and XIAP enhances anti-tumor immunity when combined with radiation and PD-1 blockade in a syngeneic model of head and neck cancer. *OncoImmunology* 7: e1471440.
48. Le, D. T., J. N. Durham, K. N. Smith, H. Wang, B. R. Bartlett, L. K. Aulakh, S. Lu, H. Kemberling, C. Wilt, B. S. Luber, et al. 2017. Mismatch repair deficiency predicts response of solid tumors to PD-1 blockade. *Science* 357: 409–413.